Multicriticality in a self-dual Potts model

1993 J. Phys. A: Math. Gen. 26 495

(http://iopscience.iop.org/0305-4470/26/3/014)

J. Phys. A: Math. Gen. 26 (1993) 495–518. Printed in the UK

Multicriticality in a self-dual Potts model

Yolanda M M Knops†, Henk W J Blöte† and Bernard Nienhuis‡

† Laboratorium voor Technische Natuurkunde, PO Box 5046, 2600 GA Delft, The Netherlands

‡ *Instituut voor Theoretische Fysica, Universiteit van Amsterdam, Valckenierstraat 65,* 1018 XE Amsterdam, The Netherlands

Received 24 July 1992, in final form 5 October 1992

Abstract. We explore the self-dual plane of a two-dimensional Potts model with vacancies and four-spin interactions, using finite-size scaling of transfer-matrix results. Since the transfer matrix construction is based on the random-cluster representation of the Potts model, its application is not restricted to an integer number q of Potts states. For $q \leqslant 4$ the self-dual plane contains a critical region belonging to the ordinary Potts universality class, and a region of first-order transition points. The two regions are separated by a line of which a range consists of Potts tricritical points, while another range is of a first-order nature. The point separating these two ranges is, for $0 < q \leqslant \frac{9}{4}$, identified with the multicritical point of which an exact solution has recently been given by Nienhuis *et al.*

1. Introduction

The normal critical point of the two-dimensional, q-state Potts model can be characterized as the end-point of the coexistence line of q phases that are related by q-fold permutation symmetry. Instead, tricritical Potts behaviour occurs when the coexistence includes not only these q phases, but also an additional phase, which is unrelated by symmetry. Such an extra phase may be introduced by means of vacancies, for instance by allowing an additional 'empty' state for each Potts variable, as was done in the renormalization analysis by Nienhuis *et al* [1]. This analysis yielded a satisfactory description of criticality, tricriticality, and first-order transitions in the Potts model. An unfortunate consequence of the introduction of vacancies is that the model is no longer self-dual. Thus, the location of the tricritical point in the Potts model with vacancies involves the determination of two unknown parameters: the first one is adjusted such that the model undergoes a phase transition, and the second one such that the transition just changes from second- to first-order.

Since a duality transformation of the Potts model on the square lattice transforms vacancies into 4-spin interactions and vice versa, it is, however, possible to construct a self-dual Potts model with both vacancies and 4-spin interactions [2]. In the 'isotropic' case (i.e. with square symmetry) the Hamiltonian is given by [17, equation (3)]. In particular we consider the random-cluster expansion of the partition function. The presence of vacancies and face variables introduces additional degrees of freedom with respect to the random-cluster model of Kasteleyn and Fortuin [3]. Apart from bond variables b_i, there are also site variables v_j and face variables f_k, describing the vacancies and the 4-spin interactions respectively. All variables have values 0 or

0305-4470/93/030495+24$07.50

1, but with the restrictions that all four b_i around a vacancy ($v_j = 0$) are equal to zero, and that all four b_i around a frozen face ($f_k = 0$) are equal to one. Hence the vertices of a frozen face must be occupied ($v_j = 1$). The Boltzmann weights are expressed using the notation of [17] as

$$\begin{aligned} u &= \mathrm{e}^{J} - 1 & A &= \mathrm{e}^{K_2} \\ P &= \mathrm{e}^{K_1} & B &= \mathrm{e}^{-J+M_2} u \\ R &= \mathrm{e}^{4J+M_1} u^{-4} \end{aligned} \tag{1}$$

where u is the bond weight, P is the weight of a vacancy, R is the weight of a frozen face, A is the weight of the nearest-neighbour vacancy–vacancy interaction and B that of a nearest-neighbour pair of frozen faces. With these substitutions the partition function can be written

$$Z_{RC}(q, u, P, R, A, B) = q^N \sum_{\{b_i, v_j, f_k\}} q^{N_l} (u/q)^{N_b} (P/q)^{N_v} R^{N_f} A^{P_v} B^{P_f} \tag{2}$$

where N is the total number of sites, N_l is the number of independent loops closed by the non-zero bond variables, $N_b = \sum_i b_i$ is the number of bond variables, $N_v = N - \sum_j v_j$ is the number of vacancies, $N_f = N - \sum_k f_k$ is the number of frozen faces, P_v is the number of nearest-neighbour vacancy pairs and P_f is the number of nearest-neighbour pairs of frozen faces. The sum in (2) contains only those terms satisfying the restrictions on neighbouring variables: a vacancy (frozen face) is surrounded by four empty (covered) edges. The self-dual manifold is characterized by

$$u = q^{1/2} \qquad P = Rq \qquad A = B. \tag{3}$$

For fixed q it is a plane parametrized, e.g. by A and P. Every point in this plane is self-dual and the plane is expected to be the locus of the phase transition between the low-temperature and the high-temperature regime. We expect to observe new universal behaviour in the self-dual plane, as we shall discuss below in some detail.

For $A = B = P = R = 0$ (2) reduces to the ordinary Potts model. Thus, for small A, B, P and R, it is plausible that the model still belongs to the Potts universality class. However, when the weight P of the vacancies (and thus that of the frozen faces) is increased sufficiently, new behaviour will occur. This behaviour will still depend on the interaction A between the vacancies, which applies, by duality, also to the frozen faces. For instance, let us introduce $P' = P^{1/4}$ and $A' = AP^{1/2}$ and consider the limit $P' \to 0$ while keeping A' fixed. In this way we inhibit interfaces between vacancies and occupied sites (and thus, because of (3), between frozen and non-frozen faces). In this case the behaviour as a function of A' is quite clear. For not too large A', the pure Potts behaviour of the model is not modified, at least not in the thermodynamic limit. The Boltzmann weights of the allowed configurations do not change. However, for some value of A', the free energy of the states dominated by vacancies or frozen faces intersects with that of the pure Potts phase and a first-order transition takes place. Continuity requires that this transition is located on a first-order line, extending to some range of non-zero values of P'.

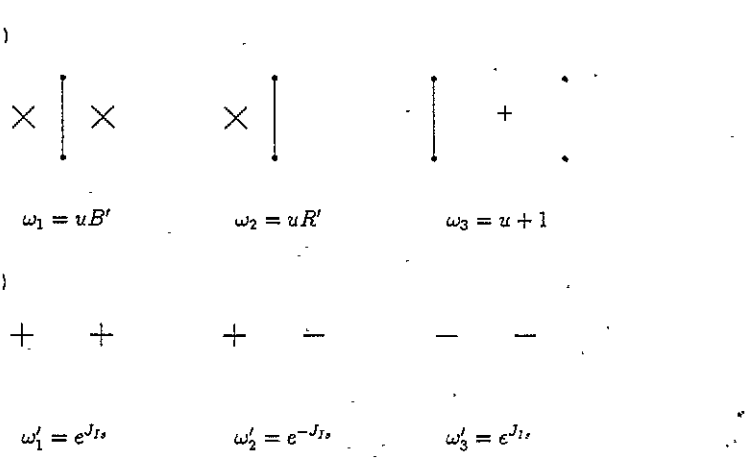

Figure 1. (*a*) Weights which are of importance in the ordered Potts state and the state dominated by frozen faces, where we have introduced $B' = BR^{1/2}$ and $R' = R^{1/4}$. Non-zero bond variables appear as lattice edges, sites as dots, and frozen faces as crosses. The plus sign on the right indicates addition of the local weights. (*b*) The corresponding Ising weights. This correspondence holds in the limit where all sites belong to a percolating cluster, i.e. $q \gg 4$ in the self-dual plane.

Here we make a distinction between two different q-ranges. For $q \leqslant 4$ the transition between the ordered and the disordered phase in the ordinary Potts model is continuous. For $q > 4$ this transition is first-order. Let us first consider the case $q > 4$. For small A, B, P and R the ordered and the disordered Potts states are in equilibrium. Therefore we expect two first-order transitions instead of one: simultaneously the ordered Potts state comes in phase equilibrium with a state dominated by frozen faces and the disordered Potts state with a state dominated by vacancies. In the first case only three vertices play a part (see figure 1(*a*)). For systems far from criticality, i.e. $q \gg 4$, the bond variables are approximately independent and can be summed out. Thus the vertices of figure 1(*a*) almost correspond with the vertices in the Ising model (see figure 1(*b*)) and we expect an Ising critical point in the neighbourhood of the point $w_2/w_1 = w_2/w_3 = \sqrt{2} - 1$. This is only an approximate location because the vertices in figure 1(*a*) interact (via the number of random cluster components) unlike the Ising vertices in figure 1(*b*). This Ising critical point is identified as the end-point of the first-order line in the self-dual plane. Moreover it is the critical end-point of an Ising line in the ordered phase bounded by the self-dual plane. By duality, there is also an Ising line in the disordered phase ending in a critical end-point coinciding with the aforementioned critical end-point. The Ising lines are the continuation of one another; but since they pertain to transitions between different pairs of phases, they are interpreted as distinct Ising lines.

For $q \leqslant 4$ it is less clear what happens at large P. Let us follow the system along a path starting from $A = 0$ at some positive constant P, such that the vacancies and frozen faces are already abundant, but do not yet percolate. Then, the occupied sites are still able to sustain the critical Potts state. It is plausible that, when A is increased, the vacancies or frozen faces will percolate continuously. This transition may be identified with the Potts tricritical one. When A (and thus also B) is further

increased, the system enters into the coexistence region of the phases in which the vacancies or the frozen faces have condensed. Furthermore, it is plausible that this tricritical line will connect to the aforementioned first-order line. The phases separated by both lines are of a similar type.

Thus, the behaviour with increasing A will depend on the starting value of P. For smaller P, the transition to the coexistence region will become more abrupt since it is increasingly driven by the pair attractions A and B. A higher-order critical point, that should perhaps be called a tri-tricritical point, may be expected where the tricritical line turns first-order. This multicritical point, which marks the end of the coexistence of the critical Potts phase with the condensed phases, is a good candidate for the interpretation of the exact solution given in [17]. However this exact solution is only critical for $0 < q \leqslant \frac{9}{4}$. Thus for $\frac{9}{4} < q \leqslant 4$ the behaviour of the phase diagram in the self-dual plane is less clear.

It is obvious that these scenarios for $q \leqslant \frac{9}{4}$ and $q > 4$, while plausible, contain some degree of speculation. For this reason we investigate the phase diagram in the self-dual plane using a numerical transfer-matrix technique. Section 2 explains the construction of the transfer matrix, in which the number q of Potts states appears as a continuous variable. Finite-size scaling ideas, useful for calculating critical exponents and the conformal anomaly are described in section 3. In section 4 we present our results, including the phase diagram and a number of critical exponents. We conclude with a summary in section 5.

2. The transfer matrix

The transfer-matrix technique used below is a generalization of that used for a study of the critical behaviour of the pure Potts model on the square lattice [4]. Thus we use the random-cluster representation of the present Potts model. We consider this model on a $L \times M$ lattice $\mathcal{L}_M$ wrapped on a cylinder, such that the finite-size parameter L is the circumference of the cylinder. The lattice $\mathcal{L}_M$ contains M rows of L sites, all faces between the first and the Mth row, and the lattice edges between nearest-neighbouring sites, but with the exclusion of those in the Mth row (figure 2(a)).

Using the weights given in section 1, the Potts partition sum $Z^{(M)}$ can be written as

$$Z^{(M)} \equiv {Z_{RC}}^{(M)}(q, u, P, R, A, B) \tag{4}$$

where the superscripts M indicate the M rows of the cylinder explicitly.

As in [4], the partition sum is divided into a number of restricted sums according to $Z^{(M)} = \sum_\alpha Z_\alpha^{(M)}$ where the index α is called a connectivity; it is determined by the bond, site and face variables on $\mathcal{L}_M$ such that it comprises the following information:

1. which sites on the Mth row are vacant,
2. which of the remaining sites on the Mth row are mutually connected by some path of non-zero bond variables on $\mathcal{L}_M$,
3. which faces between the Mth row and the $(M-1)$th row are frozen.

This is precisely the information needed for use of α as an index of the transfer matrix. A graphical illustration of a connectivity is given in the appendix (see

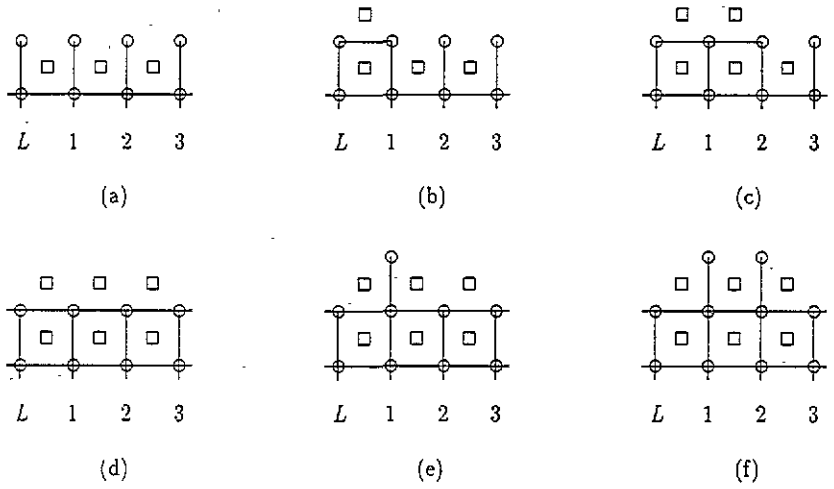

Figure 2. Illustration of the action of the sparse matrices $\mathbf{T}_i^{\mathrm{v}}$ and $\mathbf{T}_i^{\mathrm{h}}$. Bond variables appear as lattice edges, site variables as ○, and face variables as □. (*a*) The topmost row of the lattice just before the transfer matrix multiplication. The bond variables between the topmost sites have not yet been appended. (*b*) The topmost part of the lattice after the multiplication of the restricted partition sum by the sparse matrix $\mathbf{T}_1^{\mathrm{h}}$. This operation adds one new bond variable and one new face variable, and also takes into account the interaction between the site variables connected by the new bond, and that between the face variables on either side of that bond. If the new bond closes a loop, an extra weight factor q is contributed. (*c*) The same operation, but shifted over one lattice unit, is represented by the sparse matrix $\mathbf{T}_2^{\mathrm{h}}$. (*d*) The topmost part of the lattice after multiplication by the sparse matrix $\mathbf{T}_L^{\mathrm{h}}$ which completes the new rows of bond and face variables. The new row of site variables remains to be added. (*e*) The topmost part of the lattice after the multiplication of the restricted partition sum by the sparse matrix $\mathbf{T}_1^{\mathrm{v}}$. This operation adds one new vertical bond variable and one new site variable, and also takes into account the interaction between the site variables connected by the new bond, and that between the face variables on either side of that bond. (*f*) The same operation, but shifted over one lattice unit, is represented by the sparse matrix $\mathbf{T}_2^{\mathrm{v}}$.

figure A1). For actual calculations we require a representation of the connectivities by subsequent positive integers. Such an explicit evaluation of the index α as a function of the variables on $\mathcal{L}_M$ will be given in the appendix.

The action of the transfer matrix can be illustrated by appending a new row l_{M+1} to the lattice: $\mathcal{L}_{M+1} \equiv \mathcal{L}_M \cup l_{M+1}$. The Boltzmann factor associated with the new row, as well as the index β of the restricted partition sums on $\mathcal{L}_{M+1}$, depend only on α and the bond, site and face variables on l_{M+1}. Therefore the restricted partition sums on $\mathcal{L}_{M+1}$ can be expressed as a linear combination of those on $\mathcal{L}_M$

$$Z_\beta^{(M+1)} = \sum_\alpha T_{\beta\alpha} Z_\alpha^{(M)} \tag{5}$$

in which the transfer matrix $T_{\beta\alpha}$ is defined by

$$T_{\beta\alpha} = q^L \sum_{\{b_i, v_j, f_k\}|\beta,\alpha} q^{n_1} (u/q)^{n_b} (P/q)^{n_v} R^{n_t} A^{p_v} B^{p_t} \tag{6}$$

where n_l is the number of independent loops closed by the newly appended bond variables, n_b, n_v and n_f are the numbers of new non-zero bond variables, new vacancies and new frozen faces, respectively. The increase of the numbers of nearest-neighbour vacancy pairs and nearest-neighbour pairs of frozen faces is denoted as p_v and p_f respectively. The sum in (6) is over those values of the new variables that satisfy the restrictions on neighbouring variables and lead to a connectivity β on the $(M+1)$th row, given the connectivity α on the Mth row.

The transfer matrix, which extends the lattice in the vertical direction, can be decomposed as $\mathbf{T} = \mathbf{T}^{\mathrm{v}}.\mathbf{T}^{\mathrm{h}}$ where $\mathbf{T}^{\mathrm{h}}$ adds the horizontal bonds in the Mth row and the faces between the Mth and the $(M+1)$th row, and $\mathbf{T}^{\mathrm{h}}$ adds the sites on the $(M+1)$th row, and the vertical bonds between Mth and the $(M+1)$th row. The weight of the newly added sites accounts for the vacancies. The weight of the newly added bonds does not only include that of the corresponding bond variables, but also that due to the vacancy–vacancy interactions along the bonds, and interactions between the face variables at either side of each bond. In order to save memory and computer time, $\mathbf{T}^{\mathrm{v}}$ and $\mathbf{T}^{\mathrm{h}}$ are decomposed into L sparse matrices

$$\mathbf{T}^{x} = \mathbf{T}^{x}_{L}.\mathbf{T}^{x}_{L-1}.\ldots.\mathbf{T}^{x}_{2}.\mathbf{T}^{x}_{1} \tag{7}$$

where $x = \mathrm{h}$ or v, and $\mathbf{T}^{x}_{i}$ appends the ith bond with the associated site or face, taking into account the Boltzmann weights of the corresponding interactions. The matrices $\mathbf{T}^{\mathrm{h}}_{i}$ and $\mathbf{T}^{\mathrm{v}}_{i}$ are sparse: they contain at most three non-zero elements per column. Their action is illustrated in figure 2(*a*)–(*f*). After application of less than $2L$ sparse matrix multiplications, the topmost row of the lattice is incomplete. However, an adequate description of these incomplete rows requires precisely the same set of connectivities as required for complete rows: only the states of the topmost faces and sites, and the way in which the topmost sites are connected, matter. For some further details on sparse matrix decompositions, including the transformation of (7) into a product of L *identical* sparse matrices, see [4].

The free energy per site in the limit of an infinitely long cylinder ($M \to \infty$) with finite size L is determined by

$$f(L) = L^{-1} \log \Lambda^{(0)}_{L} \tag{8}$$

where $\Lambda^{(0)}_{L}$ is usually the largest eigenvalue of $\mathbf{T}$. Furthermore, the correlation length $\xi(L)$ is inversely proportional to the logarithm of the gap in the eigenvalue spectrum of $\mathbf{T}$

$$\xi^{-1}(L) = \log(\Lambda^{(0)}_{L}/\Lambda^{(1)}_{L}) \tag{9}$$

where $\Lambda^{(1)}_{L}$ is the second-largest eigenvalue of $\mathbf{T}$. In analogy with the treatment of the 'simple Whitney polynomial' in [4], the transfer matrix defined above does not keep track of magnetic correlations in the length direction of the cylinder. Thus we expect that, in the present case, the correlation length is associated with an energy-like correlation function.

The two largest eigenvalues of $\mathbf{T}$ were calculated numerically by means of the direct iteration-Hessenberg algorithm described in [4], for several values of q, and for system sizes up to $L = 9$. For $q = 1$, simplified transfer matrix calculations are possible (see the appendix), and data up to $L=14$ were obtained.

3. Finite-size behaviour

The theory of conformal invariance [5–9] provides direct relations between the finite-size amplitudes of the free energy and the correlation length, and the critical exponents. The asymptotic finite-size dependence of the free energy per site is [6]

$$f(L) \simeq f(\infty) + \frac{\pi c}{6L^2} \tag{10}$$

where c is the conformal anomaly of the model (which determines the set of critical exponents [5, 7]). Furthermore the asymptotic behaviour of the correlation length for large L is determined by [9]

$$\frac{L}{\xi(L)} \simeq 2\pi x \tag{11}$$

where x is the scaling dimension of the correlation function pertaining to ξ. Thus, x can be estimated from the scaled gap $x(L)$ defined as

$$x(L) = \frac{L}{2\pi\xi(L)}. \tag{12}$$

Renormalization group arguments [10] lead to finite-size scaling relations [11] for the free energy and the correlation length

$$f(1/L, t) = g(1/L, t) + l^{-d} f(l/L, l^{y_t} t) \tag{13}$$

$$\xi^{-1}(1/L, t) = l^{-1}\xi^{-1}(l/L, l^{y_t} t) \tag{14}$$

where y_t is the exponent of some scaling field t, l is the scaling factor and d the dimensionality of the system. The non-singular part of the transformation is denoted $g(1/L, t)$. Studying the behaviour of the scaled gap in the neighbourhood of the fixed point gives us insight into the renormalization flow. The choice $l = L$ in (14) leads to the finite-size dependence of the scaled gap $x(L, t)$ expanded in powers of t

$$x(L, t) = x + \frac{L^{y_t} t}{2\pi}\left[\frac{\mathrm{d}\xi^{-1}(1, t)}{\mathrm{d}t}\right]_{t=0} + \cdots. \tag{15}$$

Thus the relevance of t, i.e. the sign of y_t determines whether $x(L, t)$ converges to, or diverges from x for increasing L.

Differentiating (13) and (14) with respect to t and taking $l = L$ gives

$$f^{(j)}(1/L, t) = g^{(j)}(1/L, t) + L^{jy_t - d} f^{(j)}(1, L^{y_t} t) \tag{16}$$

$$\xi^{-1(j)}(1/L, t) = L^{jy_t - 1}\xi^{-1(j)}(1, L^{y_t} t) \tag{17}$$

where (j) denotes the jth derivative with respect to t.

Thus numerical evaluation of the two largest eigenvalues of T for a number of finite sizes L yields, via (8)–(11), series of estimates of c and x.

Other exponents can be obtained by numerically differentiating the free energy and the inverse correlation length. The numerical differentiation of a function F at a certain point t is performed as follows. We calculate $F(t + \Delta t)$ for $\Delta t = 0, \pm t\epsilon, \pm\frac{1}{2}\sqrt{2}t\epsilon, \pm\frac{1}{2}t\epsilon$, where ϵ fixes the interval of the numerical differentiation. Since F is analytic, we may apply a Taylor expansion

$$F(t+\Delta t) = F^{(0)}(t) + \Delta t F^{(1)}(t) + \frac{1}{2}(\Delta t)^2 F^{(2)}(t) + \cdots. \qquad (18)$$

Fitting the unknowns $F^{(i)}$ on the basis of the numerical data leads to estimates of the first and second derivative of the function F. The problem is to determine that ϵ for which the combination of errors, made by neglecting the higher-order terms in (18) and the numerical inaccuracy due to round off errors, is minimal. This minimum is estimated on the basis of a series of values of ϵ which differ, for reasons of efficiency, by a factor of $\sqrt{2}$ per step.

By fitting (16) and (17) to the data for the first and second derivative of the free energy and the inverse correlation length for a number of finite sizes L we obtain a series of estimates for the critical exponent y_t. Inaccuracies introduced by the expected corrections to scaling can be reduced by means of iterated fits, described e.g. in [12], of the series of estimates of y_t. The new series are expected to converge faster. Iterated fits are also made for the conformal anomaly c and the scaling dimension x.

4. The phase diagram

In order to determine the phase diagram in the self-dual plane, we apply finite-size scaling to results obtained by the transfer-matrix technique. At constant values of P', calculations are performed at small intervals of A'. We have located some phase transitions, and determined their nature from plots of the scaled gap versus A', for finite sizes $L \leqslant 5$. To obtain more precise locations, critical exponents and the conformal anomalies at these transitions, we have performed calculations up to $L = 9$.

The results are, in summary, as follows. We found, for values of q in the range $0 < q \leqslant \frac{9}{4}$, a Potts tricritical line which turns first-order at what may be called a tri-tricritical point. This point agrees with the locus of the exact solution presented in [17].

Also for q between $\frac{9}{4}$ and 4 we have located a first-order line and a tricritical line. The numerical data still suggest that they connect. In this range of q the exactly solvable point is not critical anymore, thus it is no longer a good candidate for the tri-tricritical point, unless that transition itself has turned first-order. However, within our numerical accuracy, we were unable to distinguish the exactly solvable point from the point where the first-order line and the tricritical line meet. Neither could we discern new structures in this neighbourhood of the phase diagram. In the absence of an exact solution describing a multicritical point, we have to conclude that the scenario proposed for $q \leqslant \frac{9}{4}$, however plausible, is not necessarily applicable to $\frac{9}{4} < q \leqslant 4$.

For q greater than 4 we have located a line of first-order transitions which ends in an Ising critical point. This point does not coincide with the exactly solvable point.

These results are summarized in figure 3, the phase diagram in the self-dual plane. Numerical evidence of these statements is given below.

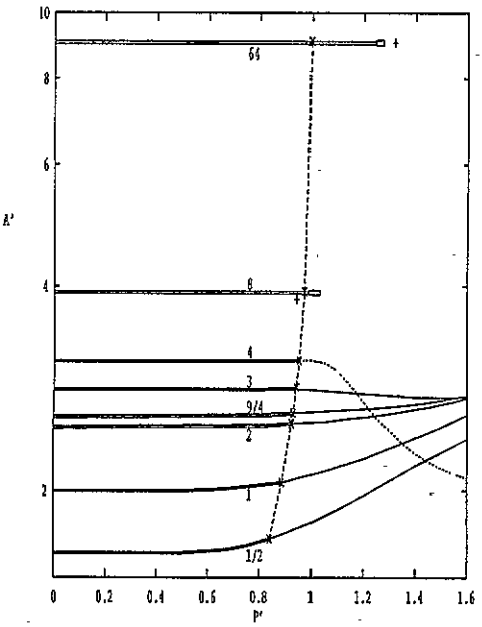

Figure 3. The phase diagram in the self-dual plane for several values of q. The curves are labelled with the pertinent q-value. The double curves denote first-order transitions, the single curves tricritical transitions. The Kosterlitz–Thouless transition for $q = 4$ is shown as a dotted curve; in this case the uncertainties of A'_{tc} are rather large due to slow finite-size convergence. The location of the exactly solved point (see [17]) is indicated by the crosses and that of the calculated Ising-like critical point (neglecting the interaction between the bonds) by the plusses. The rectangles denote the numerically determined Ising critical points; the widths of the rectangles denote the error bars.

4.1. Number of states $\leqslant 4$

4.1.1. The first-order transition. The first-order transition in the self-dual plane is one between a critical Potts state and an ordered state dominated by vacancies or frozen faces. Therefore the leading finite-size dependence of the free energy of a critical Potts state (10) has to be taken into account. The intersections of the scaled gap do not converge to zero, as usually is the case for a first-order transition. See figure 4(*a*) and 4(*b*). We have determined this scaled gap for several values of q; they are listed in table 1.

Table 1. The conformal anomaly of the critical Potts model for several values of q, determined at the first-order transition. These results are obtained from the convergence point of the intersections of the scaled gap for successive finite-sizes L in figures like figures 3 and 4. Estimated uncertainties in the last decimal places are given between parentheses. Also the analytical value for the conformal anomaly is given. These results confirm that the first-order transition is one between a critical Potts state and a non-critical one.

q	0.5	1.0	2.0	2.25	3.0	4.0
c	−0.45(1)	0.00(1)	0.50(1)	0.58(1)	0.81(1)	1.01(1)
c(exact)	−0.4458	0	1/2	0.5876	4/5	1

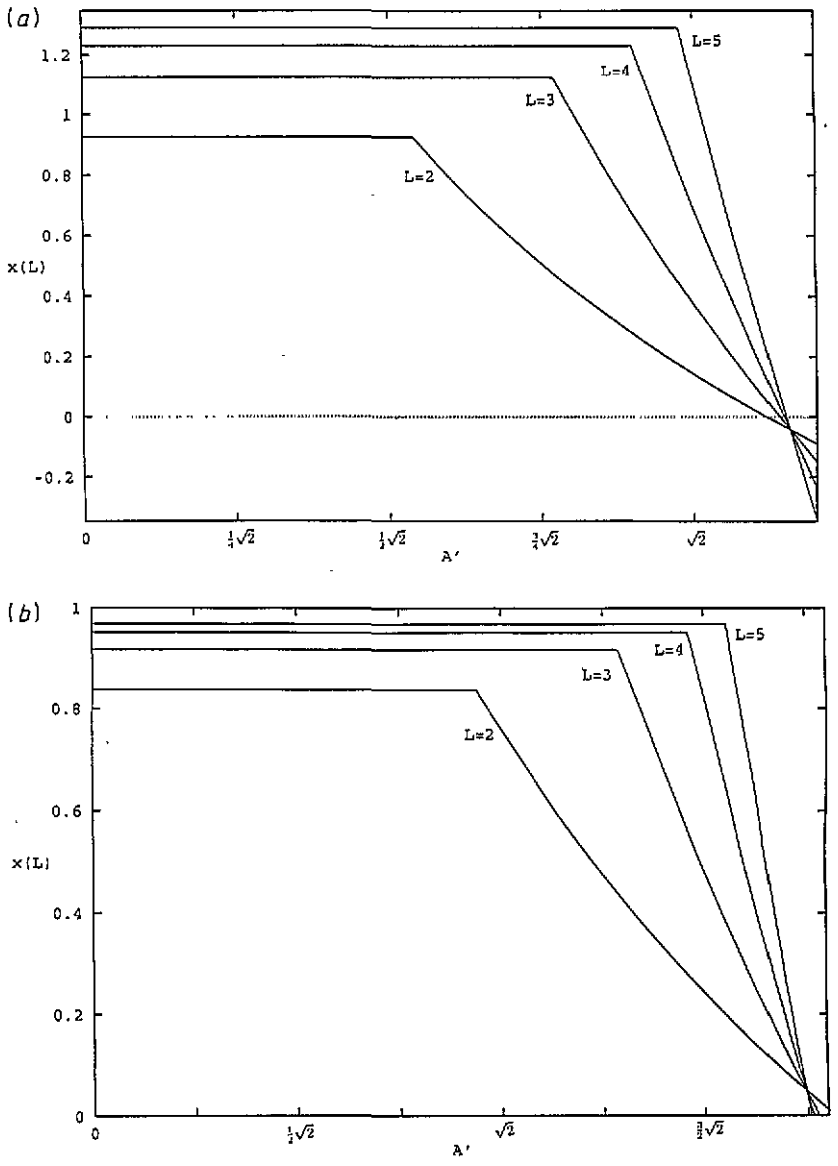

Figure 4. The scaled gap as a function of the nearest neighbour vacancies weight A'. The single vacancy weight P' is chosen as 0. The different curves represent finite sizes $L = 2$ up to $L = 5$. Data are shown for (*a*) $q = \frac{1}{2}$ and (*b*) $q = 2$. The gaps vanish at the dotted curve; a first-order transition takes place here.

This gap should be equal to $c/12$, which can be seen as follows. When A' is small, $P = 0$ inhibits vacancies or frozen faces from being present. Thus the gap is that of the pure Potts model and does not depend on A'. But when A' is increased above a certain threshold, the eigenvalue of T associated with a state with only vacancies or frozen faces will overcome the second largest eigenvalue for $A' = 0$. The scaled gap is now determined by the free energy difference between the critical Potts state and the state with only vacancies or frozen faces. The asymptotic free energy per site for

a critical Potts state is given by (10), where c is the conformal anomaly of the critical Potts model, and that for a state with only vacancies is $2 \log A'$. The scaled gap thus behaves as (see (12))

$$x(L, a) = \frac{L^2}{2\pi} a + \frac{c}{12} \tag{19}$$

where $a = f_\infty - 2 \log A'$. For $a = 0$ the system undergoes a first-order transition from a critical Potts state to a state with only vacancies or frozen faces. It follows immediately from (19) that the intersections of the scaled gaps converge to $c/12$ instead of zero. This is corroborated by the data in table 1. It also follows from this equation that, in the neighbourhood of the critical point, the slopes of the scaled gaps for systems of size L should be proportional to L^2. Analysing the data shown in figures 4(*a*) and 4(*b*) it was verified that this is the case. This behaviour is in accordance with the discontinuity fixed-point exponent $y = 2$ associated with first-order phase transitions.

4.1.2. The tricritical line. At criticality the scaled gap $x(L)$ will converge to the corresponding scaling dimension (11) with increasing finite size L . Convergence is expected to the critical leading thermal exponent x_{t1}^{c} of the ordinary Potts model for small A and P, and to the tricritical leading thermal exponent x_{t1}^{tc} at the tricritical line . From (15) and the known relevant tricritical second thermal exponents for $q < 4$ it follows that the derivatives of the $x(L)$ versus A' curves diverge. Therefore we expect intersections of these curves, converging to x_{t1}^{tc} for increasing system sizes.

This is indeed the case, as shown in figure 5(*b*). For small A the system is in a critical Potts state. The scaled gap converges to the critical Potts temperature exponent x_{t1}^{c} ($x_{t1}^{c} = 1$ for $q = 2$). The slopes of the scaled gap versus A curves are asymptotically proportional to L^y (see (15)), where $y = 2 - x$ is the renormalization exponent of the fixed point governing the flow. Thus the way in which the slope depends on the successive system sizes indicates that the renormalization flow is from the tricritical point to the critical point. Therefore the scaling exponent y_t in (15) is relevant; the scaled gap diverges from the tricritical fixed point for increasing L. For $q = 4$ (figure 5(*c*)) y_t is marginal so that the scaled gaps are parallel for successive system sizes. This result confirms the renormalization flow scenario for the dilute Potts model proposed in [1].

For $q = 1/2$ (figure 5(*a*)) we noticed that for some values of A the second-largest eigenvalue is complex, which means that the correlation function oscillates. This effect may disappear in the thermodynamic limit.

For an accurate determination of c and x_{t1}^{tc}, it is desirable to calculate f and ξ^{-1} at a point where the corrections to scaling are small. To this purpose we have selected P such that the finite-size dependence of the intersection points is small. This occurs near $P'/q^{1/4} = 1.4$. The corresponding value of A is determined as follows. Draw a horizontal line near the fixed point in figure 5(*a*) and 5(*b*). The intersections of the scaled gaps with this line will converge to A_{tc} with increasing system sizes . The nearer the horizontal line is to the scaling dimension, the better the convergence to A_{tc} is. We have used the Coulomb gas prediction for the scaling dimension x_{t1}^{tc} and solved A from $x(A, L) = x_{t1}^{tc}$. With iterated fits we have estimated A_{tc}. The results

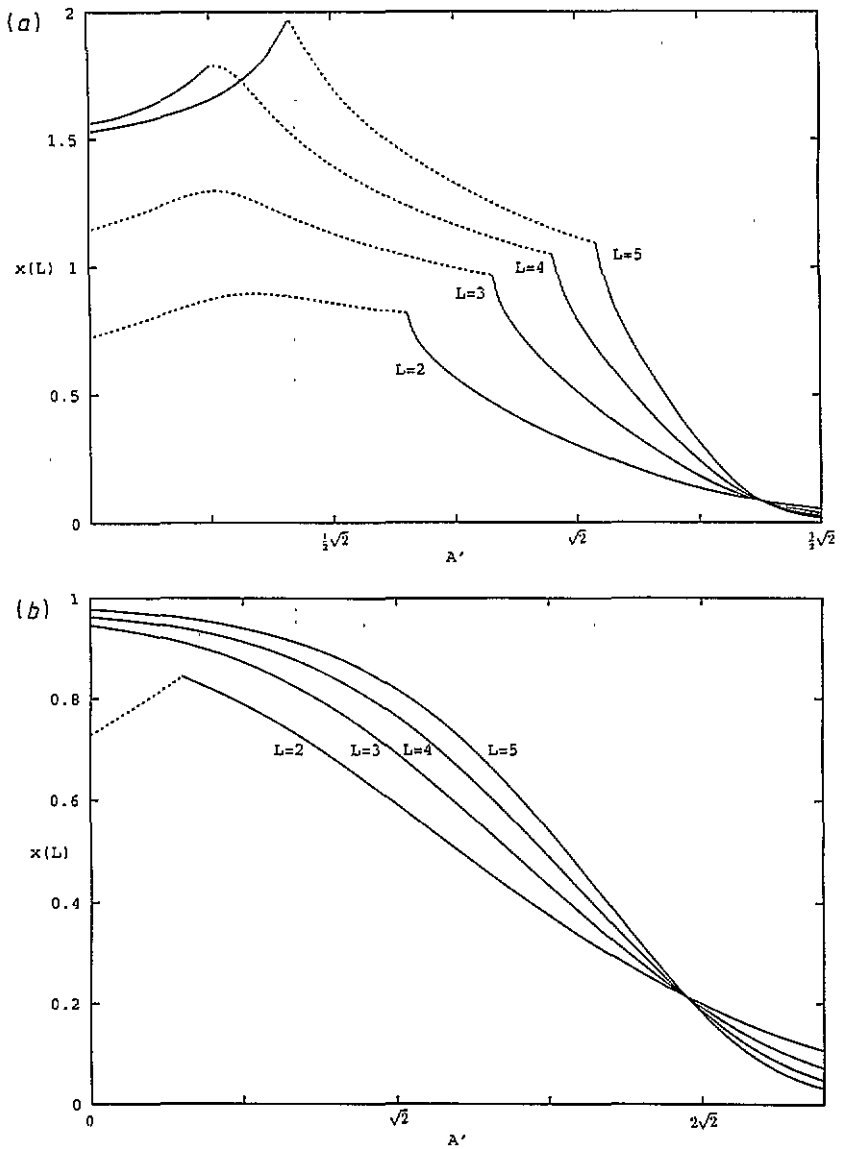

Figure 5. The scaled gap as a function of the vacancy–pair weight A'. The weight of a single vacancy $P'/q^{1/4}$ is chosen as 1.4. Data are shown for (*a*) $q = \frac{1}{2}$, (*b*) $q = 2$ and (*c*) $q = 4$. The different curves represent finite sizes $L = 2$ up to $L = 5$. For $q = 4$ data are shown up to $L = 7$; the scaled gap decreases with the finite size. The dotted curves indicate that the second eigenvalue is complex.

are shown in table 2. This way to determine A_{tc} and the tricritical exponent is not suitable for $q = 4$ because $\partial x(L)/\partial A$ does not diverge for $L \to \infty$ at tricriticality. Therefore for $q = 4$ we determined A_{tc} by requiring that the scaled gaps are parallel for two successive system sizes, i.e. the point where the second thermal exponent becomes marginal. Results from $L = 2$ to 9 and the iterated fits are shown in table 2. Free energies and scaled gaps were calculated at these points. Iterated fits

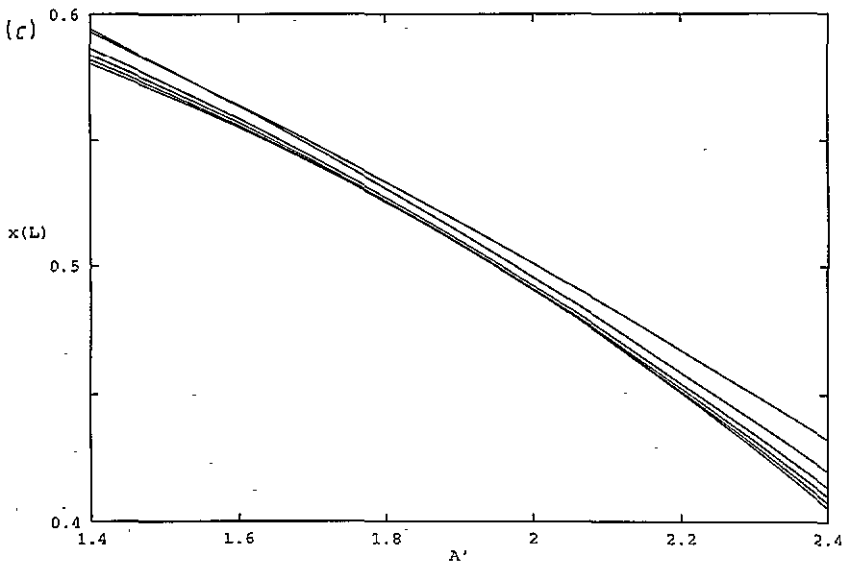

Figure 5. (Continued)

Table 2. Points at the tricritical line for several values for q where the corrections to scaling are almost minimal. For $q = 1$ we used finite-size results up to $L = 14$, for the other q values up to $L = 9$. Estimated numerical uncertainties in the last decimal places are given between parentheses.

q	A'_{tc} at $P'/q^{1/4} = 1.2$	A'_{tc} at $P'/q^{1/4} = 1.4$	A'_{tc} at $P'/q^{1/4} = 1.5$
0.5	—	1.95318(1)	2.032078(3)
1	—	2.387849(2)	2.478841(2)
2	—	2.78162(1)	2.87012(1)
2.25	—	2.82185(1)	2.90643(1)
3	—	2.81676(2)	2.88232(2)
4	2.040(2)	1.950(2)	—

Table 3. Numerical and analytical results for the conformal anomaly and the scaling dimension for the tricritical Potts model for several values of q. The numerical results are obtained with an iterated fit procedure, using the finite-size results for the free energy and the scaled gap. The transfer-matrix calculations were done at the tricritical line for $P'/q^{1/4} = 1.4$. Estimated numerical uncertainties in the last decimal places are given between parentheses.

q	c	c(exact)	x_{t1}^{tc}	x_{t1}^{tc}(exact)
0.5	0.355(3)	0.35795	0.0828(2)	0.08305
1	0.5000(2)	1/2	0.12500(5)	1/8
2	0.7000(2)	7/10	0.20000(5)	1/5
2.25	0.7420(2)	0.74184	0.21950(5)	0.21946
3	0.8572(2)	6/7	0.2857(1)	2/7
4	1.0000(2)	1	0.5000(2)	1/2

according to (10) and (11) yielded the estimates of c and x_{t1}^{tc} as shown in table 3.

The analytic expressions for the two leading thermal exponents of the Potts model

found by Nienhuis [2], using a Coulomb gas method, are

$$y_{t1} = 3 - 3t \tag{20}$$

$$y_{t2} = 4 - 8t \tag{21}$$

where

$$2\cos(\pi/2t) = -\sqrt{q}. \tag{22}$$

The conformal anomaly is given by [6, 13]

$$c = 1 - \frac{3(2t-1)^2}{t}. \tag{23}$$

Equation (22) has two solutions for t. The case $t > \frac{1}{2}$ describes the Potts critical behaviour and $t < \frac{1}{2}$ the tricritical Potts behaviour. The tricritical solution is the analytic continuation of the critical solution. The analytic predictions for c and x_{t1}^{tc} are also shown in table 3.

Table 4. Numerical and analytical data for the second thermal exponent of the tricritical Potts model for several values of q. The numerical results were obtained by an iterated fit procedure using numerical derivatives of the free energy and the inverse correlation length with respect to A. Estimated numerical uncertainties in the last decimal places are given between parentheses.

q	P'	y_{t2}^{tc} from $\xi^{-1(1)}$	y_{t2}^{tc} from $\xi^{-1(2)}$	y_{t2}^{tc} from $f^{(2)}$	y_{t2}^{tc}(exact)
0.5	1.4	1.10(2)	1.10(1)	1.10(2)	1.11192
	1.5	1.11(1)	1.11(1)	1.10(3)	—
1.0	1.4	1.000(1)	1.0000(5)	1.000(2)	1
	1.5	1.000(1)	1.0000(5)	1.0000(2)	—
2.0	1.4	0.800(2)	0.79(1)	0.800(2)	4/5
	1.5	0.800(1)	0.795(5)	0.800(2)	—
2.25	1.4	0.750(2)	0.74(1)	0.746(2)	0.74811
	1.5	0.749(1)	0.750(2)	0.747(1)	—
3.0	1.4	0.574(2)	—	0.573(2)	4/7
	1.5	0.572(1)	—	0.573(2)	—
4.0	1.4	0.0000(2)	—	—	0
	1.5	0.0000(1)	—	—	—

To obtain more exponents we have numerically differentiated f and ξ^{-1} with respect to A at the tricritical point as already determined. Using (16) and (17), and iterated fits we have found the exponent governing the crossover to ordinary Potts critical behaviour. It is identified as the second thermal exponent (21). These results are shown in table 4. No results are presented for the fits of the first derivative of the free energy. Because of the influence of the finite-size dependence of the non-singular part of the transformation (16) convergence is poor and no accurate results are obtained. For the second derivative of the free energy the finite-size dependence of the second part of the right-hand side of (16) is stronger. Thus the influence of the non-singular part decreases and we obtain good convergence.

The results in tables 3 and 4 are in perfect agreement with the predicted tricritical thermal exponents, thus confirming that we have found the tricritical line.

4.1.3. The tri-tricritical point. A number of tri-tricritical exponents was calculated exactly in [17]. Using the parametrization introduced in that paper, the exponents are

$$x^{\mathrm{tt}} = \frac{k^2 - 1}{2h(h-1)} \tag{24}$$

where

$$h = \frac{\pi}{\arccos(\Delta/2)} \tag{25}$$

with

$$q = (\Delta - \Delta^{-1})^2 \tag{26}$$

and

$$k = \frac{h}{\pi} \arccos(\Delta'/2) \tag{27}$$

with $\Delta' = 1/\Delta, -1/\Delta, -\Delta$.

As explained in [17] the Boltzmann weights are functions of Δ and q. Equation (26) gives four possible solutions for Δ, describing distinct solvable models. Thus four branches can be defined (see [17, equation (14)]). Branch 1 corresponds to the interval $\Delta \geqslant 1$, branch 2 to $0 \leqslant \Delta \leqslant 1$, branch 3 to $-1 \leqslant \Delta \leqslant 0$ and branch 4 to $\Delta \leqslant -1$. Only at branch 1 are the Boltzmann weights positive; therefore it is the only physical branch.

The numerical evaluation of the two largest eigenvalues of the transfer matrix for a number of finite sizes L yields, via (8)–(11), a series of estimates of the conformal anomaly c and an energy-like scaling dimension x. However, we have to reckon with the possibility that a scaling dimension x becomes negative, such as occurs e.g. in $O(n)$ models [12, 14, 15]. Then, the amplitude of the largest eigenvalue no longer corresponds to the conformal anomaly. Therefore it is more convenient to describe the finite-size amplitude of both 'free-energy levels' $f_i(L)$ $(i = 0, 1)$ on the same footing by appending indices i to f and c in (10), and to postpone an identification of the amplitudes in terms of c and x.

The finite-size calculations were performed for several values of q on branches 1 to 4, and for system sizes L up to $L = 9$. For $q = 1$, simplified transfer matrix calculations (see the appendix), yielded data up to $L=14$ on branches 1, 2 and 3. On branch 4, the largest eigenvalues, as obtained with the algorithm for general q, are missing in the eigenvalue spectrum of the simplified matrix.

The results were subjected to fits in accordance with (10). The accuracy benefits from the fact that $f(\infty)$ is known from the equivalence of the loop model [17, equation (28)] with the 6-vertex model solved by Lieb [16]. The reduced free energy per Potts site is

$$f(\infty) = \frac{1}{2}\log q + 2\int_0^\infty \frac{\sinh[\pi t(h-1)/h]\tanh(\pi t/h)}{t\sinh(\pi t)}\,\mathrm{d}t \tag{28}$$

with h given by (25). Best estimates in terms of c_0 and c_1 are shown in table 5, together with estimated uncertainties. The last entry for c_1 is not the analytic

Table 5. Numerical results for the finite-size amplitudes of the logarithms of the two largest eigenvalues of the transfer matrix. These amplitudes contain a factor $6/\pi$ (see (10)) so that, when appropriate, they may be interpreted as the conformal anomaly. Estimated uncertainties in the last decimal places are given between parentheses.

branch	q	c_0	c_1
1	2.25	1.003 (5)	−0.1 (1)
1	2	0.9560 (2)	−0.14 (5)
1	1.5	0.8438 (1)	−0.18 (2)
1	1	0.70000 (1)	−0.201 (1)
1	0.5	0.50000 (5)	−0.1862 (2)
1	0.25	0.35345 (5)	−0.1534 (1)
2	0.25	0.2571 (1)	−0.3251 (2)
2	0.5	0.3902 (1)	−0.4458 (2)
2	1.0	0.60000 (1)	−0.60000 (2)
2	1.5	0.7745 (1)	−0.7052 (2)
2	2.0	0.9286 (1)	−0.7856 (2)
2	2.5	1.0683 (2)	−0.8505 (5)
2	3.0	1.1972 (2)	−0.904 (1)
2	4.0	1.4300 (2)	−0.992 (1)
2	8.0	2.1600 (5)	−1.198 (1)
2	16.0	3.161 (1)	−1.387 (1)
3	16.0	3.513 (1)	−2.751 (1)
3	8.0	2.422 (1)	−3.052 (1)
3	4.0	1.5615 (5)	−3.439 (1)
3	3.0	1.2650 (2)	−3.6231 (5)
3	2.5	1.0935 (2)	−3.7455 (5)
3	2.0	0.9000 (1)	−3.9000 (2)
3	1.5	0.6750 (1)	−4.1052 (2)
3	1.0	0.4000000(1)	−4.40000 (1)
3	0.5	0.0259 (1)	−4.8953 (2)
3	0.25	−0.2523 (1)	−5.3485 (2)
4	0.25	−1.9839 (1)	−7.4794 (5)
4	0.5	−2.5568 (1)	−8.078 (1)
4	1.0	−3.8001 (2)	−9.800 (2)
4	1.5	−5.758 (1)	−7.044 (2)

continuation of the other c_1 data for branch 4: level crossing occurs between $q = 1$ and $q = 1.5$.

As is shown in [17] the numerical data for c_0 and c_1 at branch 1 are in perfect agreement with the largest two of the four theoretical amplitudes. Therefore the identification of the corresponding exponent ($\Delta' = 1/\Delta$ in (24)) as the leading thermal exponent is justified. At the other branches the computed c_0 and c_1 also agree with the theoretical amplitudes, but not always with the largest two (see [17, figure 3]).

In order to determine the exponent describing the crossover to ordinary Potts critical behaviour we numerically differentiated f and ξ^{-1} with respect to A at branch 1. Results of iterated fits are shown in table 6. The numerical values for the second thermal exponent are in agreement with the analytic exponent in (24) with $\Delta' = -1/\Delta$. Thus we have found an identification for another of these analytic exponents.

4.2. Number of states > 4

In the thermodynamic limit the ordered and the disordered Potts state are in phase

Table 6. Numerical and analytical data for the second thermal exponent of the tri-tricritical Potts point for several values of q. The numerical results were obtained by an iterated fit procedure using the data of the numerical differentiation of the free energy and the inverse correlation length with respect to A. Estimated numerical uncertainties in the last decimal places are given between parentheses.

q	y_{t2}^{tt} from $\xi^{-1(1)}$	y_{t2}^{tt} from $\xi^{-1(2)}$	y_{t2}^{tt} from $f^{(2)}$	y_{t2}^{tt}(exact)
0.5	1.790(1)	1.792(3)	1.788(2)	1.7895
1.0	1.8000(2)	1.803(2)	1.799(2)	9/5
2.0	1.81(1)	1.82(1)	1.82(3)	20/11
2.25	1.825(1)	1.822(1)	1.825(5)	1.8316

equilibrium at the self-dual plane. For finite sizes L the ordered state is more stable than the disordered state. Since the computer program calculates only the two leading eigenvalues, it fails to calculate the desired gap, namely that between the ordered Potts state and the state dominated by frozen faces (which is degenerate with the state dominated by vacancies), for most values of A' (see figure 6). If the range of A, where the right gap is calculated, is too small the location of the first-order transition cannot be found accurately. Therefore we have calculated all eigenvalues of the transfer matrix. Since this is much more time consuming we have restricted the finite sizes to $L \leqslant 5$.

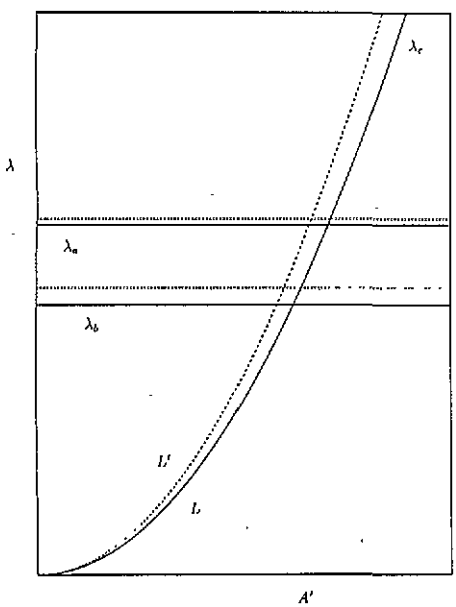

Figure 6. Schematic picture of the eigenvalues of the ordered Potts state λ_a, the disordered Potts state λ_b and the degenerate states dominated by frozen faces or vacancies λ_c as function of the nearest neighbour frozen faces weight A' for $q > 4$. The full curves are for a finite size L smaller than that of the broken curves L'. For larger finite sizes the difference between λ_a and λ_b becomes smaller, until, in the thermodynamic limit, it disappears. This figure demonstrates that, on the basis of a calculation of the two leading eigenvalues, the scaled gap between the ordered Potts state and the state dominated by frozen faces is found only in a narrow range of A' where $\lambda_a > \lambda_c > \lambda_b$.

For $q \gg 4$ and small P' we expect a first-order transition when the weights w_1 and w_3 are approximately equal (see section 1). Thus at the first-order transition the weight of A' is

$$A'_{\mathrm{fo}} \approx \sqrt{q} + 1. \tag{29}$$

From figure 7(*a*) it can be seen that this is the case. This figure is made on the basis of the two leading eigenvalues only.

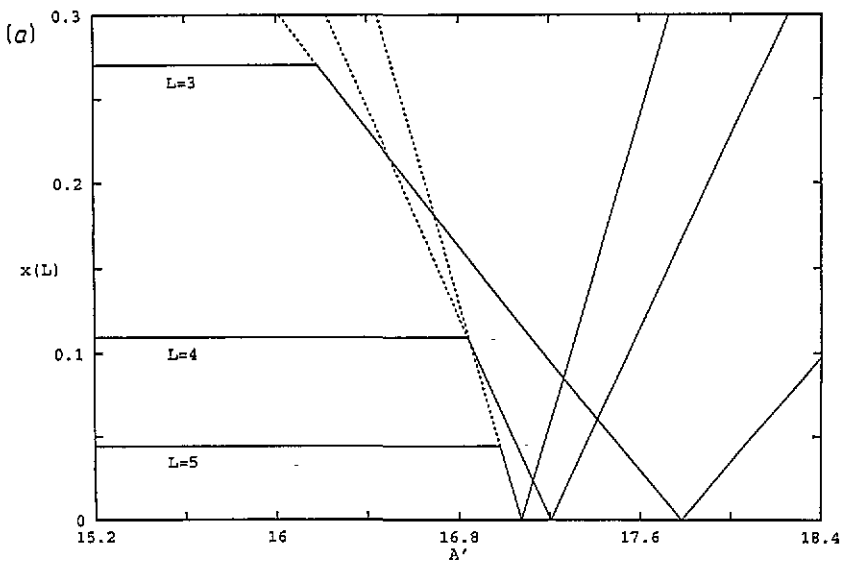

Figure 7. Scaled gaps as function of the nearest neighbour vacancies weight A' for $q = 256$. (*a*) The weight of a single vacancy P' is set equal to 0. The scaled gap is calculated for finite sizes $L = 3, 4, 5$. The horizontal parts of the full curves represent the scaled gaps between the ordered and the disordered Potts state, the remaining parts are the scaled gaps between the ordered Potts state and the state dominated by frozen faces. The full curves are obtained from the two leading eigenvalues. The broken curves represent also the scaled gaps between the ordered Potts state and the state dominated by frozen faces. They are calculated using the first and the third eigenvalue. The intersections of the broken curves converge to a scaled gap 0 and to that A' where the first-order transition takes place. (*b*) The weight of a single vacancy P' is set equal to 0.11, in the neighbourhood of which we expect an Ising critical point. The scaled gap is that between the ordered Potts state and the state dominated by frozen faces. It is calculated for finite sizes $L = 4, 5$. Here the scaled gaps behave in a way consistent with convergence to $x = \frac{1}{8}$. (*c*) Is the same as (*b*), only the weight of a single vacancy P' is set equal to 0.125.

We expect the Ising critical point in the neighbourhood of (see section 1)

$$A'_{\mathrm{Is}} = \sqrt{q} + 1$$
$$P'_{\mathrm{Is}} = (\sqrt{2} - 1)\frac{\sqrt{q} + 1}{q^{1/4}}. \tag{30}$$

Figures 7(*b*) and 7(*c*) confirm this. For $P' \approx P'_{\mathrm{Is}}$ the intersection is in the neighbourhood of the Ising exponent $x_{\mathrm{Is}} = 1/8$, and for $P' > P'_{\mathrm{Is}}$ there is no longer any intersection. These figures use data from the extended eigenvalue spectrum.

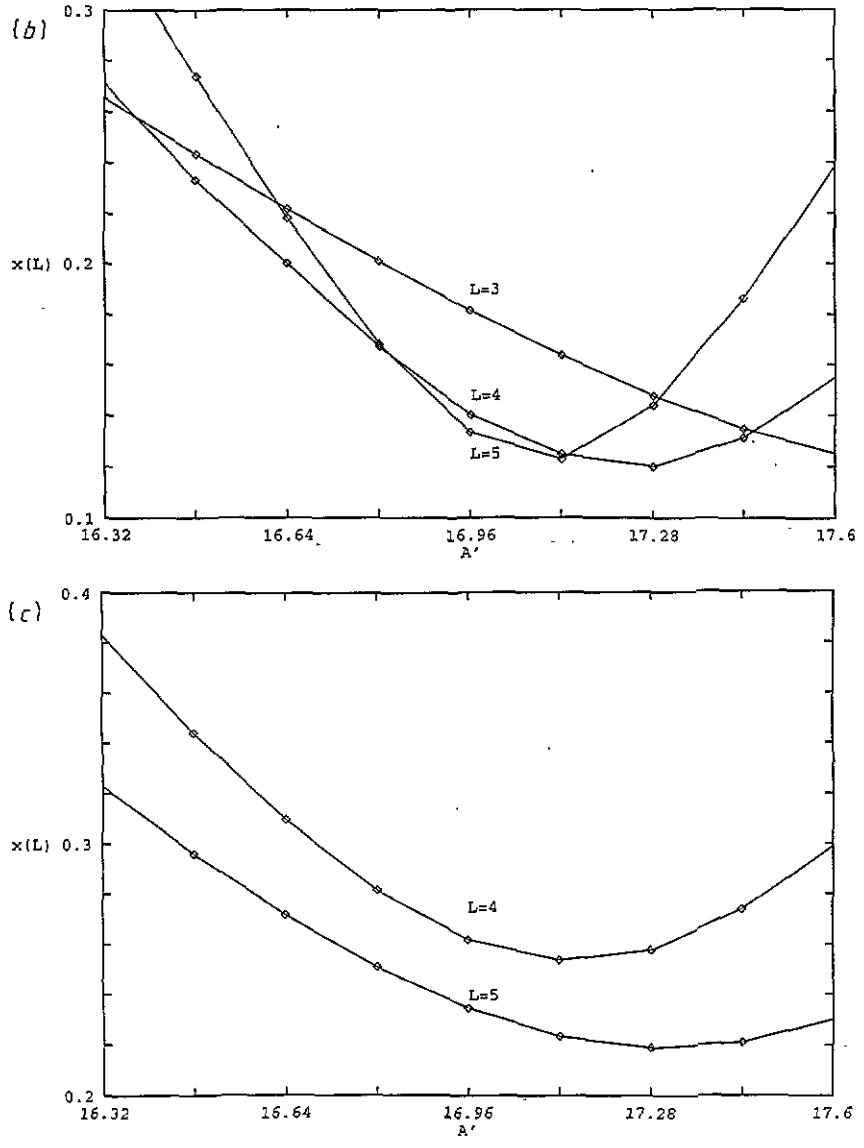

Figure 7. (Continued)

5. Conclusions

We have investigated the phase diagram in the self-dual plane of a Potts model with vacancies and 4-spin interactions by means of finite-size scaling and transfer-matrix techniques. We observe, for all q, a first-order line between a phase or phases dominated by Potts variables and phases dominated by vacancies or frozen faces. For $0 < q \leqslant \frac{9}{4}$ the transition line between the Potts states and the states dominated by vacancies or frozen faces also has a tricritical range, separated from the first-order range by a tri-tricritical point. For $q > 4$ the first-order transition ends in an Ising critical point. We have located these transitions and determined some critical

exponents and the conformal anomaly at the tricritical line and at the tri-tricritical point for several q-values.

The phase diagram in the self-dual plane for $\frac{9}{4} < q < 4$ does not seem qualitatively different from that for $q \leqslant \frac{9}{4}$. We have located a part of the first-order transition and the tricritical line, but in the absence of an exactly known multicritical point it is only approximately known where they connect. On the basis of the numerical results, we cannot exclude that the first-order line and the tricritical line connect qualitavely the same way as for $q \leqslant \frac{9}{4}$, i.e. in a tri-tricritical point. However, in that case one would expect that the exact tri-tricritical exponents found in [17] could be analytically continued for $q > \frac{9}{4}$, which is not the case. As for other possible scenarios, we can only speculate in the absence of hints from the numerical data. An obvious possibility is that the tri-tricritical point itself becomes first-order, going along the path defined by the tricritical and the first-order line. On the basis of continuity, one expects that this transition is part of another first-order line. Another possibility is that the tricritical line does not connect to the end-point of the first-order line, but to some other point of that line (in a tricritical end-point). Unfortunately, the resolving power of our computational methods is insufficient to investigate these possibilities. This remains a problem for the future.

Acknowledgments

We are much indebted to O Warnaar for valuable discussions. This research is part of the research programme of the FOM (Stichting voor Fundamenteel Onderzoek der Materie) which is financially supported by the NWO (Nederlandse Organisatie voor Wetenschappelijk Onderzoek).

Appendix. An enumeration of connectivities

The calculation of free energies and correlation lengths of $L \times \infty$ Potts models described by the partition function (2) by means of a transfer matrix for continuous values of q requires a mapping of the 'connectivities' described in section 2 on the positive integers $1, 2, 3, \ldots$. An ordering of these connectivities can be obtained using the following criteria, in decreasing order of importance:

1. the number of frozen faces,
2. the number of vacancies,
3. the positions of the frozen faces,
4. the positions of the vacancies,
5. the way in which, after elimination of the frozen faces and the vacancies, the remaining points are interconnected.

This ordering constitutes the key ingredient of an algorithm enumerating any given L-point connectivity. As a first step towards such an algorithm, we represent the connectivity (see figure A1) by means of a row of L integers $(p_1, p_2, p_3, \ldots, p_l)$ such that

1. $p_k = 0$ if and only if there is a vacancy on point k,
2. $|p_j| = |p_k|$ if and only if point j is connected to point k,
3. $p_j < 0$ if and only if there is a frozen face between point $j-1$ and point j.

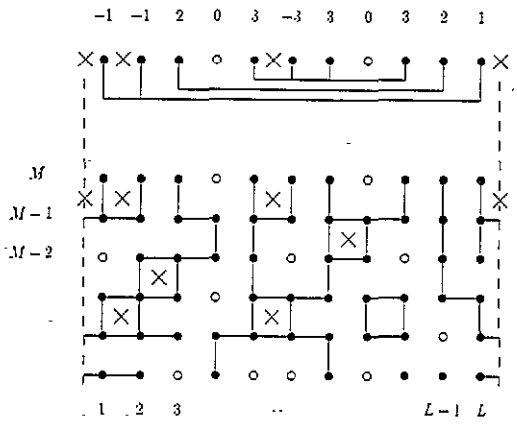

Figure A1. Illustration of the definition of the connectivities by means of an arbitrary configuration of bond, site and face variables on the square lattice with periodic boundaries (broken curves) in one direction. Vacancies are represented as open circles, occupied sites as full circles. Frozen faces are shown as crosses, faces that are not frozen are not indicated. The presence of bond variables between neighbouring sites is indicated by means of full curves. All information needed to obtain the Boltzmann weight when a new row is appended to the lattice, can be represented graphically (above). It is also shown how the connectivity can be represented by a row of integers. The same definition of the connectivities applies between the sparse-matrix multiplications described in section 2, i.e. when the topmost row is incomplete.

The coding of a connectivity by a row of integers is illustrated in figure A1. It is not a one-to-one correspondence because the choice of the absolute values of the integers is quite arbitrary. Our algorithm for the enumeration of an array of integers p_k $(k = 1, 2, \ldots, L)$ involves the definition of three auxiliary arrays:

1. An array f_j $(j = 0, 1, 2, \ldots, L - n_v - 1)$ describing the positions of the frozen faces after elimination of the points that are vacant $(p_k = 0)$. Consider an occupied point j $(p_j \neq 0)$ and let the number of vacancies $(p_k = 0)$ for $k < j$ be V_j. Then $f_{j-V_j-1} = 1$ if $p_j < 0$ and $f_{j-V_j-1} = 0$ otherwise. Since the set of distributions of the vacancies depends on whether or not the face between points 1 and L is frozen, we will consider these two cases separately. In either case the zeroth element f_0 is known, and the remaining elements are stored in the array $\boldsymbol{f} = (f_1, f_2, \ldots, f_L - n_v - 1)$ with precisely $n_f - f_0$ ones.
2. An array v_j $(j = 1, 2, \ldots, L - n_f)$ describing the positions of the vacancies after elimination of the frozen faces. Consider a non-frozen face j $(p_j > 0)$ and let the number of frozen faces $(p_k < 0)$ for $k < j$ be F_j. Then $f_{j-F_j} = 1$ if $p_j = 0$ and $f_{j-F_j} = 0$ otherwise. The case when the face between points 1 and L is frozen $(p_1 < 0)$ is special because the Lth point cannot be vacant $(p_L \neq 0)$, so that an array of length $L - n_f - 1$ suffices to code the positions of the vacancies. Adopting this choice, there are no restrictions concerning the distribution of the ones within the arrays $\boldsymbol{f}$ and $\boldsymbol{v}$.
3. An array w_j $(j = 1, 2, \ldots, L - n_f - n_v)$ describing the way in which the remaining points are connected after the elimination of the vacancies and the frozen faces. The elements are defined as $w_{j-V_j-F_j} = p_j$ for those j satisfying $p_j > 0$. An enumeration of these 'simple Whitney connectivities' is given in [4, 12].

Thus the information contained in the row p can equivalently be expressed by f_0, f, v and w. The total number of L-point connectivities with precisely n_v vacancies and n_f frozen faces is

$$N(L,n_f,n_v)=\left\{\binom{L-n_v-1}{n_f}\binom{L-n_f}{n_v}+\binom{L-n_v-1}{n_f-1}\binom{L-n_f-1}{n_v}\right\}c_{L-n_v-n_f}. \tag{A1}$$

The first term between braces is the number of ways in which the vacancies and the frozen faces can be distributed such that the face between points 1 and L is not frozen. The second term accounts for the remaining number of distributions. The factor outside the braces is the number of simple Whitney connectivities on $L-n_v-n_f$ points. It is given by [4, 12]

$$c_m=(2m)!/\{m!(m+1)!\}. \tag{A2}$$

Thus the total number of L-point connectivities is

$$a_L=\sum_{n_f=0}^{L}\sum_{n_v=0}^{L-n_f}N(L,n_f,n_v). \tag{A3}$$

Table A1. Numbers of L-point connectivities. The second column (c_L) shows the number of simple Whitney connectivities which applies to the Potts model without vacancies and face variables. The third column (b_L) contains numbers of 'simplified connectivities' which describe only the positions of the vacancies and the frozen faces, excluding the Potts degrees of freedom. They apply to the $q=1$ Potts model. The last column contains the number of connectivities derived in this appendix for the general-q Potts model with vacancies and face variables.

L	c_L	b_L	a_L
1	1	3	3
2	2	7	8
3	5	18	28
4	14	47	112
5	42	123	484
6	132	322	2200
7	429	843	10364
8	1430	2207	50144
9	4862	5778	247684
10	16796	15127	1243826

The numbers a_L are given in table A1 for some values of L, together with similar numbers for the Potts model without face variables, with and without vacancies. An enumeration of these a_L connectivities requires enumerations of the arrays f, v and w. For f and v this is simply realized by means of a function ψ acting on a row i of m integers with j zeros. This function is recursively defined as

$$\psi(i_1, i_2, \ldots, i_m) = \begin{cases} 1 & \text{if } j = 0 \text{ or } m = 1 \\ \psi(i_2, i_3, \ldots, i_m) & \text{if } i_1 = 0 \\ \binom{m-1}{j} + \psi(i_2, i_3, \ldots, i_m) & \text{if } i_1 \neq 0. \end{cases} \tag{A4}$$

An enumeration of the simple Whitney connectivities is already available by means of a function $\sigma(w)$ defined in [4]. Furthermore, we impose the rule that the connectivities with the lower number of frozen faces come first. Among connectivities with the same number of frozen faces, those with the lower number of vacancies come first. The number of connectivities which, on this ground, precede a connectivity with precisely n_f frozen faces and n_v vacancies, is

$$a_{L,n_f,n_v} = \sum_{i=0}^{n_f-1} \sum_{j=0}^{L-i} N(L,i,j) + \sum_{j=0}^{n_v-1} N(L,n_f,j). \tag{A5}$$

We can now assign a unique number α to an L-point connectivity represented by an array $p = p_1, p_2, \ldots, p_m$ with precisely n_f frozen faces and n_v vacancies. If the face between points 1 and L is not frozen, the number is

$$\alpha(p) = a_{L,n_f,n_v} + \left\{ (\psi(f) - 1)\binom{L-n_f}{n_v} + \psi(v) - 1 \right\} c_{L-n_f-n_v} + \sigma(w). \tag{A6}$$

If the face is frozen, the number is

$$\alpha(p) = a_{L,n_f,n_v} + \left\{ \binom{L-n_v-1}{n_f}\binom{L-n_f}{n_v} + (\psi(f) - 1)\binom{L-n_f-1}{n_v} + \psi(v) - 1 \right\} c_{L-n_f-n_v} + \sigma(w). \tag{A7}$$

An inverse algorithm can be defined by similar methods.

For $q = 1$, the weight of a loop in a random-cluster configuration is unity, so that one may attempt to calculate the free energy by means of a simplified transfer matrix. The degrees of freedom due to the 'simple Whitney connectivities' can be suppressed by using $\sigma(w) = 1$ and $c_L = 1$ instead of the definitions given above. This leads to a considerable decrease of the number of connectivities (see table A1) so that larger values of the finite-size parameter L come within reach. In this way one may hope to obtain a significant part of the eigenvalue spectrum of the non-simplified transfer matrix.

References

[1] Nienhuis B, Berker A N, Riedel E K and Schick M 1979 *Phys. Rev. Lett.* **43** 737
[2] Nienhuis B 1982 *J. Phys. A: Math. Gen.* **15** 199
[3] Kasteleyn P W and Fortuin C M 1969 *J. Phys. Soc. Jap. Suppl.* **46** 11

[4] Blöte H W J and Nightingale M P 1982 *Physica* **112A** 405; 1988 *Finite-size Scaling* ed J L Cardy (Amsterdam: North Holland)
[5] Cardy J L 1987 *Phase Transitions and Critical Phenomena* vol 11, ed C Domb and J L Lebowitz (New York: Academic)
[6] Blöte H W J, Cardy J L and Nightingale M P 1986 *Phys. Rev. Lett.* **56** 742
[7] Belavin A A, Polyakov A M and Zamolodchikov A B 1984 *J. Stat. Phys.* **34** 763
[8] Friedan D, Qiu Z and Shenker S 1984 *Phys. Rev. Lett.* **52** 1575
[9] Cardy J L 1984 *J. Phys. A: Math. Gen.* **17** L385
[10] Suzuki M 1977 *Progr. Theor. Phys.* **58** 1142
[11] For reviews see:
Barber M N 1983 *Phase Transitions and Critical Phenomena* vol 8, ed C Domb and J L Lebowitz (London: Academic)
Nightingale M P 1990 *Finite-size Scaling and Numerical Simulation of Statistical Systems* ed V Privman (Singapore: World Scientific)
[12] Blöte H W J and Nienhuis B 1989 *J. Phys. A: Math. Gen.* **22** 1415
[13] Dotsenko V S and Fateev V A 1984 *Nucl. Phys.* B **240** 312; 1985 *Nucl. Phys.* B **251** 691
[14] Nienhuis B 1982 *Phys. Rev. Lett.* **49** 1062
[15] Batchelor M T and Blöte H W J 1988 *Phys. Rev. Lett.* **61** 138; 1989 *Phys. Rev.* B **39** 2391
[16] Lieb E H 1967 *Phys. Rev. Lett.* **18** 1046; Lieb E H and Wu F Y 1972 *Phase Transitions and Critical Phenomena* vol 1, ed C Domb and M S Green (London: Academic)
[17] Nienhuis B, Warnaar S O and Blöte H W J 1993 *J. Phys. A: Math. Gen.* **26** 477